



HAL
open science

FluorMango, an RNA-Based Fluorogenic Biosensor for the Direct and Specific Detection of Fluoride

Claire Husser, Stéphane Vuilleumier, Michael Ryckelynck

► **To cite this version:**

Claire Husser, Stéphane Vuilleumier, Michael Ryckelynck. FluorMango, an RNA-Based Fluorogenic Biosensor for the Direct and Specific Detection of Fluoride. *Small*, In press, 10.1002/sml.202205232 . hal-03876925

HAL Id: hal-03876925

<https://hal.science/hal-03876925v1>

Submitted on 29 Nov 2022

HAL is a multi-disciplinary open access archive for the deposit and dissemination of scientific research documents, whether they are published or not. The documents may come from teaching and research institutions in France or abroad, or from public or private research centers.

L'archive ouverte pluridisciplinaire **HAL**, est destinée au dépôt et à la diffusion de documents scientifiques de niveau recherche, publiés ou non, émanant des établissements d'enseignement et de recherche français ou étrangers, des laboratoires publics ou privés.

FluorMango, an RNA-Based Fluorogenic Biosensor for the Direct and Specific Detection of Fluoride

Claire Husser, Stéphane Vuilleumier, and Michael Ryckelynck*

Nucleic acids are not only essential actors of cell life but also extremely appealing molecular objects in the development of synthetic molecules for biotechnological application, such as biosensors to report on the presence and concentration of a target ligand by emission of a measurable signal. In this work, FluorMango, a fluorogenic ribonucleic acid (RNA)-based biosensor specific for fluoride is introduced. The molecule consists of two RNA aptamer modules, a fluoride-specific sensor derived from the *crcB* riboswitch which changes its structure upon interaction with the target ion, and the light-up RNA Mango-III that emits fluorescence when complexed with a fluorogen. The two modules are connected by an optimized communication module identified by ultrahigh-throughput screening, which results in extremely high fluorescence of FluorMango in the presence of fluoride, and background fluorescence in its absence. The value and efficiency of this biosensor by direct monitoring of defluorinase activity in living bacterial cells is illustrated, and the use of this new tool in future screening campaigns aiming at discovering new defluorinase activities is discussed.

an impressive level by riboswitches, a class of RNA motifs mostly found in the 5' untranslated regions of some bacterial messenger RNAs (mRNAs). These sequences are able to specifically switch their structure in the presence of a target ligand, usually a small molecule, in order to control downstream gene expression (transcription or translation).^[1–4] Riboswitches usually comprise two domains: a sensor aptamer that specifically recognizes a target molecule (with an affinity sometimes exceeding that of antibodies for their antigen), and a regulatory platform that remodels a region of the mRNA to modulate its transcription and/or its translation. The two domains are usually functionally connected by a transducing element, also called communication module.^[1] Their modular structure makes riboswitches an excellent starting point for molecular engineering. For instance, exchanging the

sensor aptamer domain for another one, natural or synthetic, already enabled the development of engineered riboswitches for application in living cells as well as in cell-free systems.^[5–7] Thus, using such a construct to control the expression of a reporter gene (e.g., coding for a fluorescent protein, luciferase or another reporting enzyme), would yield a biosensor, that is, a biological molecule (or system) that converts the presence of a specific molecule into a measurable signal.^[8]


Among the wide palette of potential target ligands for this technology, small negatively charged molecules are expected to be the most difficult to target using RNA-based sensors as they offer only a low number of possible interaction sites and because strong electrostatic repulsion with polyanionic nucleic acids is anticipated. Fluoride, the smallest and the most electronegative anion, represents an extreme case in this context. However, its toxicity and often-problematic levels in drinking water make it a highly relevant target for specific detection.^[9] Fluoride is also a potential degradation product of fluorinated compounds, an emerging class of persistent and toxic chemicals.^[10] Specific detection of this ion would be useful in the development of high-throughput activity assays for the discovery of defluorination enzymes, of which only a few are currently known.^[11] To be applicable, a corresponding sensor should be biocompatible, highly selective, easy to use, non-toxic, commercially available or easy to produce, and generate a fluorescent signal compatible with very high-throughput screening pipelines.^[12] At present, fluoride is detectable by fluoride-specific electrodes^[13,14] or colorimetry,^[15,16] but none of these approaches fulfills all the above-mentioned requirements.

1. Introduction

Nucleic acids are central to life, playing an essential role at all stages of genetic information expression and processing. In some cases, the function of a nucleic acid involves its coding capacity (e.g., deoxyribonucleic acid and messenger ribonucleic acid). However, the great structural plasticity of these molecules is also the source of complex, often highly dynamic tridimensional structures that support highly complex cellular processes, including the catalysis of specific reactions or the specific recognition of molecular targets. In particular, the structural modularity and flexibility of ribonucleic acid (RNA) are exploited at

C. Husser, M. Ryckelynck
CNRS, Architecture et Réactivité de l'ARN
Université de Strasbourg
UPR 9002, 2 allée Konrad Roentgen, Strasbourg 67000, France
E-mail: m.ryckelynck@unistra.fr

S. Vuilleumier
CNRS, Génétique Moléculaire, Génomique, Microbiologie
Université de Strasbourg
UMR 7156, 4 allée Konrad Roentgen, Strasbourg 67000, France

 The ORCID identification number(s) for the author(s) of this article can be found under <https://doi.org/10.1002/smll.202205232>.

© 2022 The Authors. Small published by Wiley-VCH GmbH. This is an open access article under the terms of the Creative Commons Attribution License, which permits use, distribution and reproduction in any medium, provided the original work is properly cited.

DOI: 10.1002/smll.202205232

A plethora of fluorogenic chemicals, for instance, exploiting the preferential reactivity of silyl or boronic groups with fluoride has also been described,^[16–19] but none of these compounds is currently commercially available, and most of them have only limited compatibility with biological conditions (e.g., solubility in aqueous media), restricting their direct application for fluoride detection. Although counterintuitive at a first glance, RNA-based biosensors thus represent an attractive alternative in a biological context.^[1] Indeed, the aptamer domain of *crcB* riboswitches specifically recognizes fluoride and switches its structure accordingly^[20] through a mechanism in which magnesium cations (Mg^{2+}) are instrumental in mediating fluoride/RNA interactions.^[21] The *crcB* riboswitch was recently repurposed into a fluoride biosensor to control transcription of the light-up RNA aptamer Broccoli or of mRNAs coding for the green fluorescent protein (GFP) or for the catechol (2,3)-dioxxygenase.^[22] Produced transcripts can also be detected using Cas13a-based technology, further increasing detection sensitivity.^[23,24] These new biosensors proved to be very efficient in aqueous solution, with a detection limit compatible with monitoring of drinking water.^[8] Yet these systems rely on cell-free extracts or purified proteins,^[22] and on expensive fluorogenic RNA analogues.^[23,24] Moreover, such rather complex systems are efficient for highly sensitive single point measurements but less well-suited for direct analysis of fluoride and monitoring its production in solution.

Simpler biosensors for direct detection of fluoride can be obtained by directly connecting the sensor aptamer to a light-up RNA aptamer, a reporting domain that specifically recognizes a small molecule called a fluorogen, and forms a highly fluorescent complex with it.^[25–28] This interaction strongly relies on structural integrity of the aptamer. Placing the proper folding of a key element (e.g., a helix near the fluorogen-binding site) under the allosteric control of the structure switching sensor aptamer yields a fluorogenic RNA-based biosensor (FRB), as previously developed by us and others.^[1,29,30] Exploiting this concept, we completely revisited the structure of the *crcB* aptamer and the way it is used for applications requiring direct and specific fluoride detection. By fusing it with the light-up RNA aptamer Mango-III,^[31,32] we created the first fluoride-specific FRB combining the advantages of chemical (i.e., direct measurement of fluoride) and RNA-based sensors (i.e., biocompatible and safe to use molecules). This biosensor is easy to apply in any laboratory because its production and use requires only commercially available reagents. It approaches the performance of previous fluoride biosensors and enables to monitor defluorinase activity in real time.

2. Results and Discussion

2.1. First Prototype of a Fluoride-Responsive Fluorogenic RNA-Based Biosensor

To design a fluoride-specific fluorogenic RNA-based biosensor (FRB, **Figure 1A**), we used the fluoride-specific aptamer domain of the riboswitch found upstream the coding region of the *Thermotoga petrophila* *crcB* gene as sensor module.^[20] This small 52-nucleotide RNA (**Figure S1A**, Supporting Information)

folds into two helices (P1 and P2) spaced by a pair of asymmetric internal loops. The longest loop (i.e., residues 14 to 23 on **Figure S1A**, Supporting Information) forms a pseudoknot (dots lines in **Figure S1A**, Supporting Information) with the 5'-overhang sequence (i.e., residues 2 to 5). Additional long-range interactions are established by residues of the smallest loop. Taken together, these elements and interactions form a pocket able to specifically accommodate fluoride in complex with three magnesium ions, while strongly discriminating other halides.^[21] The key involvement of 5'- and 3'-overhang sequences in RNA folding and interactions with fluoride as well as their opposite orientation in the crystal structure (**Figure S1A**, Supporting Information) makes them unsuitable for engineering into a communication module. In contrast, the P2-L2 stem-loop is more attractive for this purpose. This element is proposed to fold early^[33] and the L2 loop projects away from the fluoride-binding pocket, making this motif appealing to insert an additional domain without interference with ligand binding as long as the P2 stem can still form.

As reporting module, we chose Mango-III (**Figure S1B**, Supporting Information). This light-up RNA aptamer specifically recognizes and activates the fluorescence of the fluorogen Thiazole Orange1-biotin (TO1-biotin).^[31,32] The aptamer folds in a complex pseudoknot-like structure built around a G-quadruplex forming the base of the fluorogen-binding pocket. On the other side, this binding pocket is capped by the apical $A_{15}-U_{22}$ base-pair (numbered according to **Figure S1B**, Supporting Information).^[32] The G-quadruplex is also stabilized by a base triple ($A_{12} \cdot U_{24} \cdot A_{30}$), connecting it to helix P1 (**Figure S1B**, Supporting Information). The formation of P1 is required for Mango-III function. Yet, this helix still tolerates sequence variations provided that its structure is preserved. Therefore, it is possible to use it as a connection element to the *crcB*-derived aptamer. Furthermore, as expected for a reporting module that is part of a fluoride biosensor, the presence of up to 1 mM sodium fluoride (NaF) does not affect the fluorescence of Mango-III/TO1-biotin complex (**Figure 1B**).

Taken together, these observations suggested that a fluoride-specific FRB could be generated by merging Mango-III and a *crcB*-derived aptamer at the level of their P1 and P2 helices, respectively (**Figure 1A**; **Figure S1**, Supporting Information). To rule out possible folding interference between the two domains, we first generated a construct in which both aptamers were connected via the four apical base pairs of the Mango-III P1 stem (5'-₄ACGA₇-3'/5'-₃₂UCGU₃₅-3'), yielding *crcB*-MIII (**Figure S1C**, Supporting Information). The C_4A mutation was also introduced in *crcB* to ensure good transcription yields, together with a compensatory mutation $G_{15}U$ to preserve formation of the pseudoknot. *CrcB*-MIII displayed the same capacity to activate TO1-biotin fluorescence than Mango-III alone (**Figure 1B**), confirming that the structure of the reporter module was preserved in the fusion. However, the construct fluorescence remained unchanged irrespective of the presence of fluoride, likely because of the stability of the connecting helix (in red on **Figure S1**, Supporting Information), preventing structure switching to take place. To favor responsiveness of the molecule to fluoride, we replaced the connecting helix by 5'-AUUU-3'/5'-AUUU-3' (*crcB*-AUUU-MIII, on **Figure S1D**, Supporting Information), a sequence we previously identified

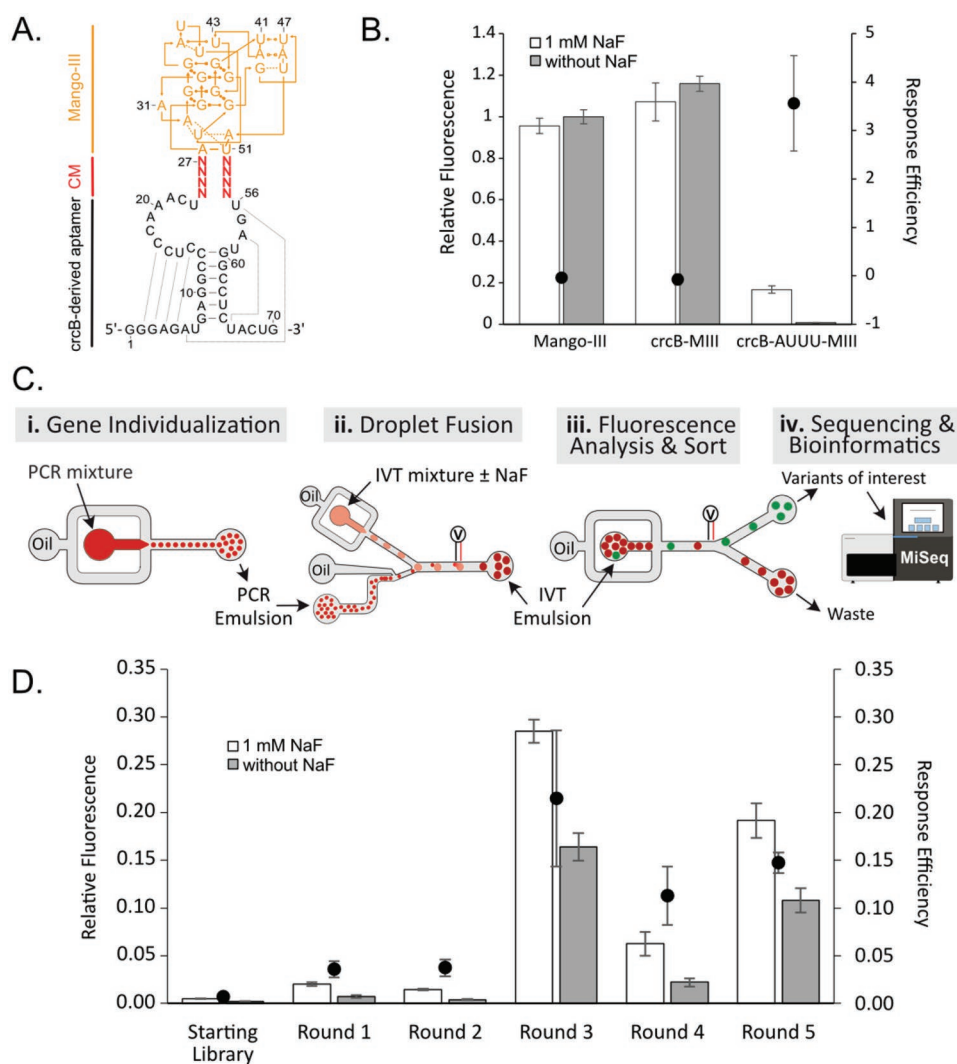


Figure 1. Selection of an RNA-based fluoride biosensor from a randomized library using μ IVC-Seq. A) Secondary structure of the starting library. A *crcB*-derived RNA aptamer (black) was fused to the Mango-III aptamer (orange) by two stretches of four randomized nucleotides (red Ns), some of which were expected to behave as communication modules (CM). Base pairs are represented according to Leontis-Westhof classification.^[47] B) Impact of fluoride on the fluorescence of Mango-III and its derivatives. Purified RNAs were incubated with (white bars) or without (gray bars) 1 mM sodium fluoride (NaF) prior to measuring the fluorescence of the RNA/TO1-biotin complex and normalizing it to that of Mango-III/TO1-biotin in the absence of fluoride. Response efficiency (dots) was calculated as described in the Experimental Section. Values are the mean of three independent experiments, and error bars correspond to ± 1 standard deviation. C) μ IVC-seq screening strategy. The different libraries were screened in a four-step process as follows: C-i) genes diluted into a PCR mixture were individualized in water-in-oil droplets prior to PCR amplification. C-ii) An in vitro transcription medium (IVT) containing the fluorogen (TO1-biotin) and supplemented or not with NaF was added to each PCR-amplified droplet by droplet fusion. C-iii) Upon gene transcription, droplets of interest were sorted according to their fluorescence. C-iv) Last, the sequences recovered after each round of screening were determined by next generation sequencing (NGS) and bioinformatics. D) Functional validation of the rounds of screening. Libraries were in vitro transcribed in the presence of TO1-biotin and in the presence or not of NaF, and fluorescence was measured and normalized by that of Mango-III in the absence of fluoride. Response efficiency of each library (dots) was calculated. Values are the mean of three independent experiments, and error bars correspond to ± 1 standard deviation.

as an efficient communication module in the context of other FRBs.^[34] Although much less fluorescent than the stabilized constructs (Mango-III and *crcB*-MIII), *crcB*-AUUU-MIII displayed a significant, ≈ 3.5 -fold increase in response efficiency to fluoride (see calculation in Experimental Section) (Figure 1B). This key metric not only considers the turn-on amplitude of a probe (i.e., the fluorescence amplitude measured in response to the addition of fluoride), it also takes into account its fluorescence efficiency (i.e., how close the fluorescence of the probe

complexed with its ligand is to the maximal fluorescence measured with Mango-III alone). To display the desired elevated response efficiency, a sample (an individual variant or a library) should not only display low fluorescence background in the absence of fluoride but also fluorescence levels in the presence of fluoride as close as possible to that of Mango-III, two key features required for an efficient FRB. Therefore, whereas *crcB*-AUUU-MIII demonstrates the potential of the construct in reporting the presence of fluoride by TO1-biotin fluorescence

emission, there is still room for improving its response efficiency.

2.2. Screening of the Library for Optimized Fluoride-Responsive FRBs

The communication module is the key element of an FRB. It should destabilize the reporter enough to keep it as silent as possible in the absence of fluoride, while the presence of fluoride should make the construct as fluorescent as possible. To identify an optimal communication module, and thus an optimal FRB, we fully randomized the connecting region over its eight positions (Figure 1A; Figure S1E, Supporting Information) prior to functional screening of the library by microfluidic-assisted In Vitro Compartmentalization in tandem with high-throughput sequencing (μ IVC-Seq).^[35] Briefly, the DNA sequence for each variant placed under the control of the T7 RNA polymerase promoter was diluted into a PCR amplification mixture prior to individualization into small 2.5 picolitre (pL) water-in-oil droplets (Figure 1C). Following PCR amplification, each small droplet was fused one-to-one with a larger one (175 pL) containing an in vitro transcription (IVT) mixture supplemented with TO1-biotin fluorogen and, depending on the selection round, with 1 mM NaF. After a last incubation step, droplets were reinjected and sorted according to their fluorescence, especially that of TO1-biotin (Figure S2, Supporting Information). At the end of each round, selected droplets were broken, and contained DNA recovered and used to prime a new round of screening. To favor enrichment of the library in molecules displaying low fluorescence in the absence of fluoride and high fluorescence in its presence, screenings were performed in two regimes. During positive selections (rounds 1, 3, and 5 on Figure S2, Supporting Information), the IVT mixture contained 1 mM NaF and only droplets displaying high green fluorescence were recovered (boxed in red on Figure S2, Supporting Information). At this stage, not only variants of interest (i.e., those requiring the presence of fluoride to become fluorescent) were recovered but also those RNAs that, similar to *crcB*-MIII, had a stable connecting helix and were fluorescent without addition of fluoride. To deplete the library from such false positive variants, rounds of positive selection were alternated with rounds of negative selection (rounds 2 and 4 in Figure S2, Supporting Information) during which no NaF was added to the transcription mixture and only droplets displaying a low green fluorescence were recovered (boxed in red in Figure S2, Supporting Information).

The response efficiency of the library was determined at the end of each round. Whereas it did not significantly improve in the two first rounds of screening (likely due to the low stringency of the sorting gates used; see Figure S2, Supporting Information), a jump in response efficiency was observed after the third round of selection that was maintained until the end of the process. No further improvement of the library was observed after the fifth round of screening, and we decided to stop the process and analyze the sequence content of the library by sequencing and bioinformatics by the previously reported μ IVC-seq approach.^[35] We identified 326 sequences out of the 65 536 initially contained in the starting library.

Detailed analysis of the enrichment capacity of each variant throughout the screening process allowed \approx two-thirds of them to be clustered as a function of the applied selective pressure (Figure S3, Supporting Information), the remainder showing a more erratic behavior. In particular, 40 sequences (termed class I variants) displayed progressive and continuous enrichment throughout both positive and negative selection regimes, as expected for an FRB. Other sequences, in contrast, showed other types of behavior. Specifically, 34 sequences showed enrichment upon rounds of positive selection only (class II variants), and 120 other sequences (class III variants) showed the opposite behavior.

2.3. Identification and Characterization of the Selected Fluoride-Specific FRB

The ten most attractive class-I variants (i.e., the best enriched and most abundant; Table S1, Supporting Information) were rapidly evaluated by fluorescence monitoring of in vitro transcribed templates in the presence of TO1-biotin, and in the presence or absence of 1 mM NaF. The six best RNAs (CM3, 6, 7, 8, 9, and 10) were then produced and purified for further analysis (Figure 2A). All displayed a strong fluorescence in the presence of fluoride and limited background signal in its absence. Moreover, three of them (CM7, 8 and 9) displayed a >13-fold response efficiency, far exceeding that of our original prototype *crcB*-AUUU-MIII (<4-fold on Figure 1B). CM7 and CM9 showed a significant variation of the fluorescence signal at NaF concentrations higher than 5 mM that compromised their full evaluation (Figure S4, Supporting Information). Proper understanding of this intriguing phenomenon would require additional experiments that are beyond the scope of the present work. On the contrary, the dose-response characterization highlighted CM8 as an optimal biosensor with an apparent dissociation constant (K_D) of $202 \pm 12 \mu\text{M}$ (Figure 2B), a value close to that reported for the aptamer found in the *T. petrophila* *crcB* riboswitch (K_D of $134 \pm 9 \mu\text{M}$).^[21] CM8 was named FluorMango (Figure 2C) and further analyzed in detail. As a result of its affinity for fluoride, FluorMango was able to reliably detect fluoride concentrations as low as $68 \mu\text{M}$ and to quantify the ion above $90 \mu\text{M}$ (linear range from 150 to 1 mM) (Figure 2D). The response of the biosensor was rather fast as fluorescence emission was detected immediately upon fluoride addition and plateaued within a few minutes (Figure S5A, Supporting Information). As expected for a chimera, the molecule also inherited the salt dependence of its two parents. Indeed, to be functional, the biosensor required potassium (a cation essential to stabilize the G-quartet fold of Mango-III) at a concentration slightly higher than that necessary for the light-up aptamer (Figure S5B, Supporting Information), likely due to the lower intrinsic structural stability of the sensor. Like most RNAs, FluorMango also requires magnesium ions (Mg^{2+}) to stabilize its structure and more importantly to mediate fluoride recognition (Figure S5C, Supporting Information), each fluoride ion forming a complex with three Mg^{2+} .^[21] Accordingly, optimal response of the biosensor was observed in 100 mM KCl and 10 mM MgCl_2 , a condition used for all measurements performed along this study. The complex formed between the biosensor and its

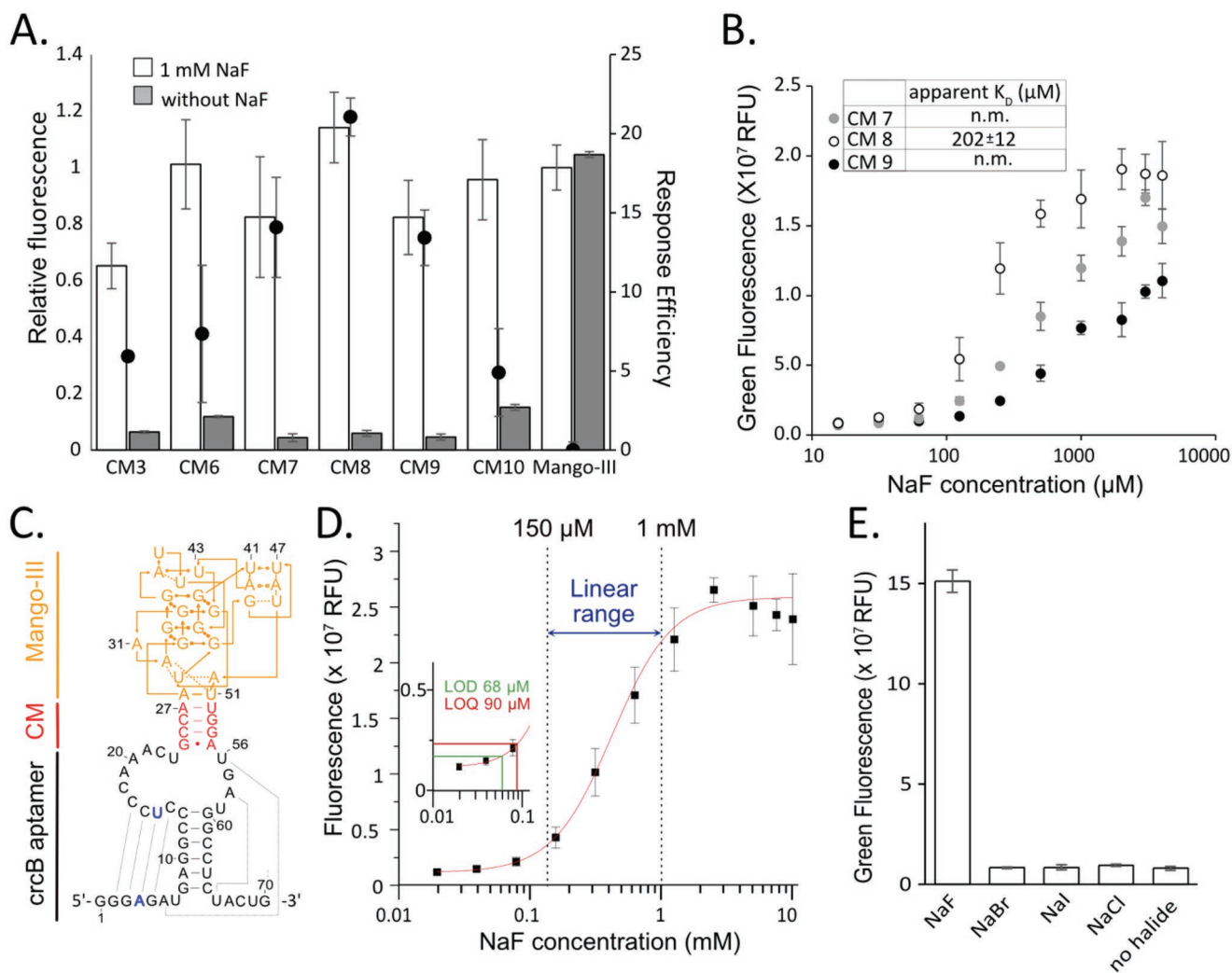


Figure 2. Identification and functional characterization of fluoride biosensors. A) Response of purified RNAs to fluoride. The most promising RNAs identified by bioinformatic analysis were produced by *in vitro* transcription and purified. 400 nM of RNA was then incubated with 700 nM TO1-biotin in the presence (white bars) or absence (gray bars) of 1 mM sodium fluoride (NaF). After 60 min, green fluorescence of the RNA/TO1-biotin complex was measured and normalized to that of Mango-III/TO1-biotin in the absence of fluoride. Response efficiency was calculated as described in the Experimental Section. Values are the mean of three independent experiments, and error bars correspond to ± 1 standard deviation. Sequences of the communication modules of tested variants are provided in Table S1, Supporting Information. B) Determination of the apparent dissociation constant (K_D) of three RNA candidates. Purified RNAs were incubated with a range of NaF concentrations, and fluorescence of the RNA/TO1-biotin complex was measured. The K_D value was calculated by fitting the data to a Hill equation when possible. Non-measurable (n.m.) values are also indicated. C) Secondary structure of the fluoride RNA-based biosensor FluorMango (CM8). The selected communication module (CM) sequence is shown in red, the reporter module Mango-III in orange, and the sensor module *crcB* aptamer in black. Positions mutated to improve the transcription rate that preserves the formation of the pseudoknot are shown in blue. D) Fluoride detection by FluorMango. Limit of detection (LOD), limit of quantification (LOQ), and linear range of fluoride detection by FluorMango were determined as described elsewhere.^[36] 400 nM of RNA was incubated in the presence of a range of NaF concentrations prior to measuring fluorescence of RNA/TO1-biotin complex. Values are the mean of seven (no NaF) or three (other NaF concentrations) independent experiments, and error bars correspond to ± 1 standard deviation. LOD was derived from three times the standard deviation, and LOQ from ten times the standard deviation. E) Specificity of FluorMango. 400 nM of purified RNAs was incubated with 1 mM of the specified halide, and fluorescence of the FluorMango/TO1-biotin complex was measured. Values are the mean of three independent experiments, and error bars correspond to ± 1 standard deviation.

ligands (i.e., fluoride and TO1-biotin) displayed excellent stability up to 28 °C before starting to melt and completely lose its fluorescence above 40 °C (Figure S5D, Supporting Information). This melting was slightly faster with the biosensor than with Mango-III, again consistent with its lower intrinsic structural stability of the former. However, the effect was completely reversible, and returning to a lower temperature (e.g., 24 °C)

fully restored fluorescence. Last of all, our sensor also displays a remarkable specificity for fluoride because no fluorescence was observed in the presence of any other halide (Figure 2E), as also observed previously for the *Pseudomonas syringae* *crcB* riboswitch.^[20]

The response efficiency and dynamic range of FluorMango mainly result from its optimized communication module.

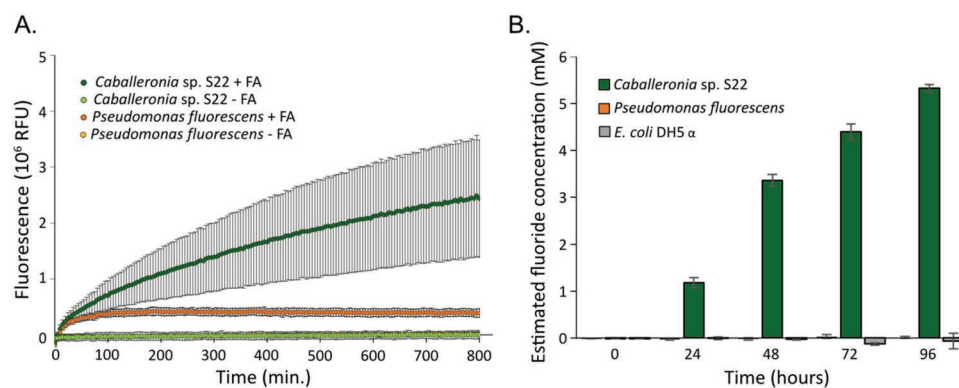


Figure 3. Defluorinase activity of different bacterial strains. A) Real-time monitoring fluoride release by *Caballeronia* sp. S22 and *P. fluorescens*. Both strains were grown to stationary phase in the presence of fluoroacetate to induce defluorinase expression in *Caballeronia* sp. S22. Then, bacteria were washed, and the same number of cells was incubated in M9 medium supplemented in refolding buffer (40 mM Tris-HCl pH 8.1, 100 mM KCl, and 10 mM MgCl₂) in the presence of FluorMango, TO1-biotin, proteinase K, with (+FA) or without (-FA) fluoroacetate. Fluorescence of FluorMango/TO1-biotin was directly monitored at 30 °C in microtiter plates. Values are the mean of three independent experiments, and error bars correspond to ± 1 standard deviation. B) Fluoride release in culture supernatants of *Caballeronia* sp. S22, *P. fluorescens*, and *E. coli*. Strains were grown in minimal medium supplemented with 1 mg mL⁻¹ sodium fluoroacetate. Samples were taken at different times, centrifuged, and supernatants were recovered. The free fluoride contained in the medium was quantified by mixing supernatant aliquots with refolding buffer supplemented in FluorMango, TO1-biotin, and proteinase K. Fluoride concentration was then calculated by comparing measured fluorescence to a calibration curve prepared with a range of NaF concentrations. Values are the mean of three independent experiments, and error bars correspond to ± 1 standard deviation.

Surprisingly, the sequence of this module is very close to that of *crcB*-MIII, which did not show any response to fluoride (Figure 1B). The two molecules have identical GC content over the three apical base pairs of their respective communication modules, with just an inverted GC pair (G₂₆-C₅₃ and C₂₆-G₅₃ in *crcB*-MIII and FluorMango, respectively) that was not expected to affect the stability of the helix. The main difference is at the level of the basal base pair, in which the canonical A₂₄-U₅₅ interaction is replaced by a non-canonical G₂₄-A₅₅ pairing. Although additional structural characterization would be required to firmly conclude, it is very likely that the local widening induced by this purine-purine pair occurring right above the fluoride binding site sufficiently distorts the helix to affect the overall structural stability of the connecting helix essential to stabilize the G-quadruplex that supports Mango-III function.

2.4. Monitoring Defluorinase Activity Using FluorMango

As a first direct application of FluorMango, we used it to monitor defluorinase activity directly from living bacteria. Only a handful of defluorinases have been identified so far, among which fluoroacetate dehalogenases represent a well-characterized subclass.^[11] These enzymes were mainly isolated from bacteria living in soils contaminated by fluoroacetate, a compound naturally produced by some plants and also used industrially as rodenticide (compound 1080).^[37] The model bacterium *Caballeronia* sp. S22 (formerly known as *Pseudomonas fluorescens* DSM8341)^[38] and a *P. fluorescens* control strain (deprived of fluoroacetate dehalogenases activity) were grown in minimal medium supplemented with fluoroacetate to induce defluorinase synthesis. Pelleted and washed bacterial cultures were incubated at 30 °C (a temperature at which the biosensor displays nearly intact performance) in phosphate buffer saline supplemented or not with 1 mg mL⁻¹ fluoroacetate, and

containing 100 mM KCl, 10 mM MgCl₂, 40 mM Tris-HCl pH 8.1, 400 nM FluorMango, 700 nM TO1-biotin, and 2 U mL⁻¹ molecular biology grade proteinase K to remove potential traces of RNase activity. These conditions preserved the functionality of the biosensor for extended incubation times with no significant degradation of the molecule observed (Figure S6A, Supporting Information). Moreover, the biosensor largely conserved its performance at the chosen incubation temperature (Figure S5D, Supporting Information). No fluorescence was detected in the absence of fluoroacetate (Figure 3A). In contrast, strong fluorescence was observed with cell suspensions of the *Caballeronia* strain in the presence of fluoroacetate, and only background fluorescence was observed with the control *P. fluorescens* strain, likely because of the presence of free fluoride in the used fluoroacetate preparation (Figure S6B, Supporting Information).

To simulate the conditions of functional screening for defluorinase activity in microtiter plate format, we grew the different strains at 28 °C in minimal medium supplemented with 1 mg mL⁻¹ fluoroacetate⁻¹, taking supernatant samples every 24 hours for analysis of fluoride production as described above for grown cultures. Performing measurements in M9 medium supplemented in KCl and MgCl₂ had only very limited impact on the performance of the biosensor (Figure S7A, Supporting Information). As expected, fluoride production was only observed for *Caballeronia* sp. S22 with fluoroacetate dehalogenase activity, even after extended incubation of up to 96 h (Figure 3B). The accuracy of our observations was confirmed by repeating the experiment and comparing the results with those of a commercial colorimetric assay (Figure S7B, Supporting Information). Taken together, our data demonstrate the efficiency and robustness of our new RNA-based fluoride biosensor for accurate monitoring of bacterial defluorination activity in a direct and specific manner.

Last, we adapted our droplet-based microfluidic pipeline to the screening of bacteria for their capacity to degrade fluoroac-

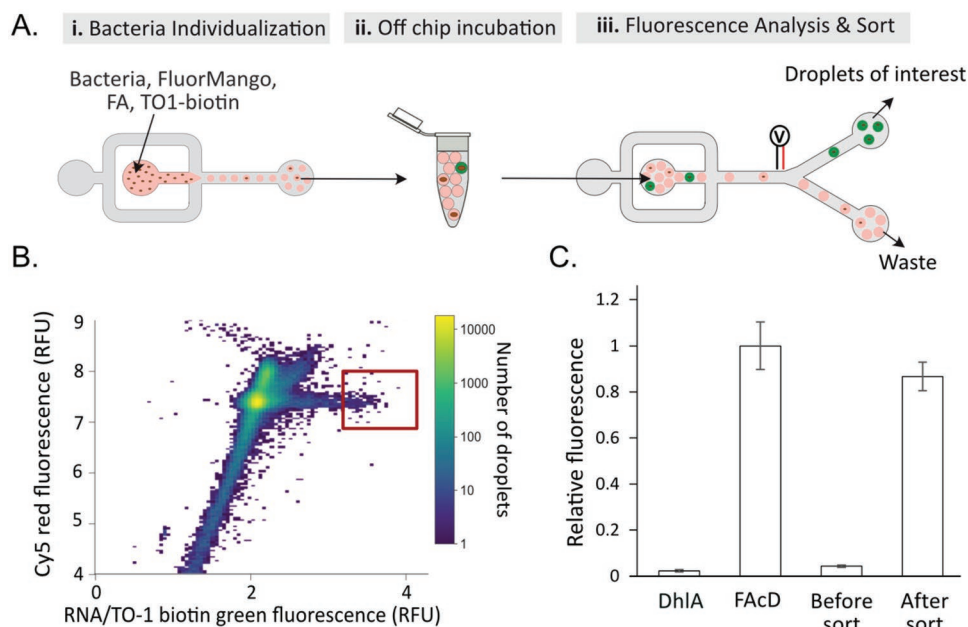


Figure 4. Screening of bacteria for defluorinase activity. A) Microfluidic screening strategy. A mixed bacterial population (1 FAcD for 99 DhIA producing strains) was screened in a three-step process as follows: A-i) bacteria were diluted into a refolding buffer supplemented with 1 mg mL⁻¹ sodium fluoroacetate, purified RNA FluorMango, TO1-biotin, and proteinase K individualized in water-in-oil droplets. A-ii) The emulsion was incubated off-chip at 30 °C prior to A-iii) sorting droplets according to their fluorescence. B) Fluorescence profile of droplets analyzed during the screening. Green fluorescence of RNA/TO1-biotin complex and Cy5 red fluorescence (droplet tracer) were measured, and droplets containing elevated green fluorescence (so high fluoride concentration) were sorted (red box). C) Validation of the round of screening. Plasmids were extracted from sorted and unsorted bacteria and used to transform *E. coli*. The same number of cells was incubated in PBS supplemented with refolding buffer in the presence of FluorMango, TO1-biotin, proteinase K, and 1 mg mL⁻¹ fluoroacetate. Fluoride production was monitored in real time for 12 h at 28 °C in a microtiter plate. The fluorescence appearance rate of the RNA/TO1-biotin complex was normalized to that of a control condition with a strain transformed by pure FAcD-coding plasmid.

etate and release fluoride. We prepared a model library made of two top ten *Escherichia coli* strains transformed either with a pBAD plasmid carrying the gene coding for the FAcD fluoroacetate dehalogenase from *Burkholderia sp.* FA1,^[39] or with the same plasmid carrying the gene coding for DhIA, a dechlorinase from *Xanthobacter flavus* strain UE15 unable to use fluoroacetate as substrate.^[40] Strains were grown and heterologous gene expression induced, prior to adding a 1/99 (FAcD/DhIA) ratio into a reaction mixture containing fluoroacetate, FluorMango, TO1-biotin, and the required cations. Bacterial dilution was adjusted to achieve 20% droplet occupancy and an emulsion was prepared as described previously (Figure 4A).^[41] Upon overnight incubation at 30 °C, the emulsion was reinjected into a sorting device and droplets displaying high green fluorescence (FluorMango in complex with fluoride and TO1-biotin) were recovered (red boxed population on Figure 4B). Bacteria contained in unsorted and sorted droplets were recovered and grown prior to extracting their plasmid DNA. Fresh bacteria were then transformed by each plasmid mixture (i.e., before and after sort) and assayed for their capacity to convert fluoroacetate into fluoride in the presence of FluorMango, TO1-biotin, and the required cations (Figure 4C). The bacteria prepared from the sorted sample displayed a 20-fold increase in defluorination activity, nearing that of a pure strain expressing FAcD, demonstrating the success of the applied selection. This phenotypic assay was further confirmed by quantitative PCR using primers targeting DhIA and FAcD coding genes, and an ≈60-fold enrichment in FAcD gene was observed after

droplet sorting (Table S2, Supporting Information). These two independent measurements validated our new pipeline and confirmed that FluorMango could be used in future screening campaigns aiming at searching for new (or improved) defluorinase activities.

3. Conclusion

Our work demonstrates that a small synthetic RNA molecule can be designed to adopt a 3D fold enabling the specific recognition of the small and electronegative fluoride in a magnesium-mediated manner, similar to what happens with the *crcB* riboswitch. Fusing this module to the light-up RNA Mango-III via carefully chosen connecting sequences allowed us to develop FluorMango, to the best of our knowledge, the first RNA-based direct fluoride biosensor reported so far. This engineering required the selection of an efficient communication module that properly balances the stability of the molecule to render the reporter highly fluorescent in the presence of fluoride, while keeping it non-fluorescent in the absence of the target. This was greatly facilitated by using our ultrahigh-throughput μ IVC-seq pipeline that allowed us to screen more than 65,000 sequence permutations for the desired functionality. Unexpectedly, converting a single canonical base-pair into a non-conical purine-purine pairing was sufficient to reach this goal, further highlighting the relevance of using an ultrahigh-throughput screening pipeline without a priori prediction.

FluorMango is less suited than Cas13a-assisted technologies for detecting trace amounts of fluoride in a sample (e.g., drinking water). Indeed, the Cas13a-mediated signal amplification makes these technologies over an order of magnitude more sensitive than FluorMango (Table S3, Supporting Information). Nevertheless, our biosensor offers several important advantages. First, the biosensor tolerates high concentrations of fluoride and enables reliable quantification of up to 5 mM fluoride, whereas polymerase-assisted approaches may be strongly inhibited by fluoride at concentrations above 100 μM (as reported for SPRINT).^[23] Second, FluorMango proportionally converts a fluoride-binding event into fluorescence emission in a direct manner. This feature not only allows fluoride quantification by end-point measurements but also enables to monitor enzyme kinetics in a straightforward manner over extended incubation times. Exploiting this feature, we showed that enzyme activity can be monitored from living cells (environmental and lab strains) both in high-throughput microtiter plate assays and in ultrahigh-throughput regime using droplet-based microfluidics. Such measurements would have been extremely complex to perform with transcription-based assays that are only compatible with endpoint measurements. FluorMango therefore expands the molecular toolbox by filling a technical gap.

The direct quantification of fluoride enabled by FluorMango in aqueous medium under biologically relevant conditions made possible by our biosensor, together with its specificity and ease of production, should render it attractive for many applications. We acknowledge that conditions that challenge RNA integrity (such as RNase activity) may somewhat restrict the application scope of FluorMango. However, adding proteinase K in the reaction mixture was found to preserve RNA in our experiments. Alternatively, our biosensor could be encapsulated into lipid vesicles that would enable fluoride to enter while preventing RNase access to the biosensor.^[42] Another solution would consist in converting FluorMango into a biosensor made of non-natural nucleotides resistant to enzymatic degradation. Several such modifications have now been described in the literature,^[43] and the μIVC -Seq pipeline could easily be adapted to search for an optimized variant of such a modified biosensor. FluorMango could also be produced in living cells by the transcription machinery and used to sense the flux of fluoride entering the cells, as nicely shown with the Broccoli-derived biosensor responding to silver.^[44]

In the present work, we started to explore the use of FluorMango to monitor defluorinase activity directly in living bacteria. The results collected in this study show that the biosensor can be used as a read-out in a μIVC pipeline (or any other ultrahigh-throughput screening approach) repurposed to search for cells displaying defluorinase activity. Therefore, exploiting this concept, it will be possible to set-up screening campaigns aiming at discovering new or improved defluorinases directly from cells (e.g., using the RAPID approach)^[45] or from in vitro expressed mutant gene libraries. Such a screening would be complex to implement using existing colorimetric assays in microtiter plate format.^[15] The fluorogenic and biocompatible FluorMango biosensor represents an attractive solution to set up screening campaigns to search for enzymes capable of degrading compounds such as polyfluoroalkylated

substances (PFAS), a class of toxic pollutants requiring urgent attention.^[10]

4. Experimental Section

Materials: All oligonucleotides used in this study (Table S4, Supporting Information) were synthesized by Integrated DNA Technologies (IDT). *Caballeronia* sp. S22 strain was obtained from DSMZ (strain DSM 8341, German Collection of Microorganisms and Cell Cultures), *E. coli* DH5 α was bought from New England Biolabs (NEB 5-alpha electrocompetent *E. coli* #C2989K), and *P. fluorescens* was a laboratory stock.

Library Preparation: The starting library DNA template was synthesized with eight randomized positions using the “hand mixing” option, allowing an expected average representation of each base (A, T, C, and G) of 25% at each position; and thus, comprising 65536 (4^8) unique variants. The library (0.1 pmol) was PCR-amplified in 100 μL of SsoFast EvaGreen Supermix (Bio-rad) supplemented with 20 pmol of Ampli-Forward (designed to introduce the T7 RNA polymerase promoter) and 20 pmol of Ampli-Reverse primers, and the mixture was thermocycled as described previously.^[34] The obtained PCR product was used to seed a second identical PCR reaction but containing 20 pmol Add-barcode primer (insert 20 randomized nucleotides acting as Unique Droplet Identifier, UDI, upstream the construct)^[35] and 20 pmol Ampli-Reverse primer. PCR product was finally purified using the Sera-Mag Select kit (Cytiva).

Microfluidics-Assisted Functional Screening: Microfluidic chips were prepared as described before,^[46] and the three main steps of the screening were performed as follows:

Digital Droplet PCR: A dilution of purified DNA (calculated to reach the desired droplet occupancy) was prepared in 200 $\mu\text{g mL}^{-1}$ total yeast RNA (Ambion) before addition to a PCR medium containing SsoFast EvaGreen Supermix (Bio-Rad) at the recommended concentration, 0.1% Pluronic F68 (Sigma), 0.2 μM of each primer (Ampli-Barcode and Ampli-Reverse), and 1 μM of Cyanine 5 (Cy5; red-fluorescence droplet tracer). The resulting solution was injected into a droplet generator device and dispersed into 2.5 pL droplets in a Novec 7500 fluorinated oil phase (3 M) containing 3% surfactant to stabilize the emulsion. The emulsion was collected and thermocycled to allow DNA amplification.^[35]

Droplet Fusion: Addition of in vitro transcription medium and RNA production was done. An in vitro transcription medium (IVT) containing 25 mM MgCl_2 , 40 mM Tris-HCl pH 8.1 (at 37 $^\circ\text{C}$), 50 mM KCl, 5 mM DTT, 1 mM spermidine, 1.6 mM of each rNTP (Larova), 17.5 $\mu\text{g mL}^{-1}$ T7 bacteriophage RNA polymerase (produced in the laboratory),^[46] 0.1% Pluronic F68, 1 μg pyrophosphatase (Roche), 200 nM TO1-3PEG-Biotin Fluorophore (ABM), 0.1 μM Cy5, and ± 1 mM NaF (Sigma) was injected into a droplet fusion device and dispersed in 17.5 pL droplets in Novec 7500 oil phase supplemented with 2% surfactant. Droplets containing PCR-amplified DNA were re-injected into the chip through another inlet and synchronized one-to-one with an IVT droplet before fusing them by applying an electric field (700 V, 30 kHz). The emulsion was collected at 4 $^\circ\text{C}$ and then placed for 2 h at 37 $^\circ\text{C}$ (positive selection) or 15 min at 37 $^\circ\text{C}$ (negative selection). Incubation time was extended during positive selection to favor variants with a stable signal over time.

Droplets Sorting and Recovery of Genes of Interest: Droplets were reinjected into a droplet sorting device mounted onto a thermoplate (Tokai) set at 40 $^\circ\text{C}$ to favor the isolation of stable RNAs and spaced with a surfactant-free Novec 7500 oil phase. Red (Cy5, droplet tracer) and green (RNA/TO1-biotin complex) droplet fluorescence were analyzed, and the droplets of interest were sorted by applying an electric field (1200 V and 30 kHz) to deflect droplets of interest into the “sort” channel. The emulsion was then broken with 100 μL of 1H,1H,2H,2H-Perfluoro-1-octanol (Sigma-Aldrich), and the aqueous phase was mixed with 100 μL of 200 $\mu\text{g mL}^{-1}$ total yeast RNA (Ambion).

Enrichment Validation and Regeneration of the Library: Recovered DNA libraries and single variants were PCR-amplified as above using Ampli-Forward and Ampli-Reverse primers (Table S4, Supporting Information)

and obtained PCR products were in vitro transcribed in the presence of 200 nM TO1-Biotin and ± 1 mM NaF for 2 h at 37 °C as before. Development of green fluorescence ($\lambda_{\text{ex}} = 510$ nm and $\lambda_{\text{em}} = 550$ nm) was monitored every minute on a microplate reader (SpectraMax iD3, Molecular Devices). Response efficiency was computed using Equation (1):

$$\text{Response efficiency} = \frac{\text{Fluo}^{+\text{NaF}} - \text{Fluo}^{-\text{NaF}}}{\text{Fluo}^{-\text{NaF}}} \times \frac{\text{Fluo}^{+\text{NaF}}}{\text{Fluo}^{\text{Mango-III}}} \quad (1)$$

where $\text{Fluo}^{+\text{NaF}}$ and $\text{Fluo}^{-\text{NaF}}$ are the fluorescence of the sample (variant or library) in the presence and absence of NaF, respectively, and $\text{Fluo}^{\text{Mango-III}}$ is the fluorescence of Mango-III in the presence of NaF.

After each round of screening, UDI barcodes were reset to preserve their uniqueness.^[35] To do so, 1 μL of the DNA template contained in the recovered aqueous phase was diluted in 100 μL PCR mixture prior to reamplifying it by PCR using Add-barcode and Ampli-Reverse primers (Table S4, Supporting Information) as above. PCR products were purified using the Sera-Mag Select kit (Cytiva).

Sequence Analysis of the Enriched Libraries: After each validated round of screening, DNA in the aqueous phase recovered from sorted droplets was amplified using Ampli-Barcode and NGS-Reverse primers to append P5 and P7 sequences subsequently used for molecular indexing using the Nextera Indexing kit (Illumina) as recommended by the supplier. PCR products were purified using the SPRIselect system (Beckman Coulter) prior to quality check by capillary electrophoresis (Bioanalyzer, Agilent). Following quantification by Qubit (Thermo Scientific), obtained libraries were analyzed on a V3-150 chip (Illumina) by MiSeq sequencing device (Illumina). The resulting reads were analyzed using a script written in Python 3 language as described elsewhere.^[35]

RNA Preparation and Purification: DNA templates were PCR-amplified using Ampli-Forward and Ampli-Reverse primers. PCR products were transcribed after mixing them with 25 mM MgCl_2 , 40 mM Tris-HCl pH 8.1 (at 37 °C), 5 mM DTT, 1 mM spermidine, 1.6 mM each of rNTP and T7 RNA polymerase and an incubation for 2 h at 37 °C. The obtained RNA was extracted using phenol/chloroform and purified by preparative gel electrophoresis as described previously.^[34]

RNA Analysis: RNA characterization was performed using 400 nM RNA in refolding buffer (10 mM MgCl_2 or as specified, 40 mM Tris-HCl pH 8.1 (at 37 °C), 100 mM KCl or as specified, 700 nM TO1-biotin). Fluorescence of RNA/TO1-biotin complexes ($\lambda_{\text{ex}} = 510$ nm and $\lambda_{\text{em}} = 550$ nm) was recorded every minute on a microplate reader (SpectraMax iD3, Molecular Devices) set at 28 °C. Three types of characterization were performed:

Response to Fluoride: RNA was incubated with or without 1 mM NaF in 50 μL refolding buffer. Formation of RNA/TO1-biotin complex fluorescence was monitored over 30 min, and its rate was computed from the slope of fluorescence through time for each condition. Response efficiency was calculated using Equation (1).

Affinity: RNAs were incubated with a range of NaF concentrations in 50 μL refolding buffer and formation of RNA/TO1-biotin complex fluorescence measured as above. For calculation of the limits of detection and quantification, experiments without NaF were repeated seven times to determine the standard deviation of the blank.

Specificity: CM8 (FluorMango) RNA was incubated with 1 mM NaF, NaBr, NaI, NaCl in 50 μL refolding buffer, and fluorescence measured as above.

Thermal Stability: CM8 (FluorMango) and Mango-III RNAs were incubated with or without 1 mM NaF in 20 μL refolding buffer, and the fluorescence of the RNA/TO1-biotin complex was measured on the FAM channel (450–490 nm) of a CFX96 Touch Real-Time PCR Detection System (Bio-Rad). Following 30 min of incubation at 24 °C, the temperature was increased incrementally by 2 °C steps, and the fluorescence of the complex was measured after 10 min of incubation at each temperature.

Monitoring Fluoroacetate Degradation by Cells: *Caballeronia* sp. S22 and *P. fluorescens* were grown at 28 °C and 110 rpm for 24 h in M9 medium (5.6 g L^{-1} Na_2HPO_4 , 3 g L^{-1} KH_2PO_4 , 1 g L^{-1} NH_4SO_4 , 0.05% glucose, 20 μg L^{-1} vitamin B1, 1 mM MgSO_4 , and 0.1 mg mL^{-1}

L-leucine) supplemented with 1 mg mL^{-1} sodium fluoroacetate (MP biomedical). Cells were pelleted, washed with phosphate buffer saline, resuspended in the same buffer, diluted to 0.5 absorbance at 600 nm, and incubated for 12 h in refolding buffer with or without 1 mg mL^{-1} sodium fluoroacetate, 400 nM purified FluorMango, 700 nM TO1-biotin, and 2 U mL^{-1} proteinase K on a microplate reader (SpectraMax iD3, Molecular Devices) set at 28 °C, recording green fluorescence ($\lambda_{\text{ex}} = 510$ nm and $\lambda_{\text{em}} = 550$ nm) every 5 min.

To detect fluoride release in culture supernatants, *Caballeronia* sp. S22, *P. fluorescens*, and *E. coli* strain (NEB 5-alpha electrocompetent *E. coli* #C2989K) were grown in minimal medium supplemented with 1 mg mL^{-1} sodium fluoroacetate. Samples were taken at different times, centrifuged, and supernatants were recovered. Free fluoride contained in the medium was quantified by mixing supernatant aliquots with 400 nM FluorMango, 700 nM TO1-biotin, and 2 U mL^{-1} molecular biology grade proteinase K. FluorMango/TO1-biotin fluorescence was then measured as above. Solutions with ranges of NaF concentrations in M9 medium supplemented in refolding buffer were prepared and measured in parallel to convert measured fluorescence to fluoride concentration (Figure S7A, Supporting Information).

Microfluidics-Assisted Bacterial Defluorinase Activity Screening: A pBAD plasmid containing the DhIA-coding gene was provided by Prof. D. Janssen.^[40] The DNA fragment coding fluoroacetate dehalogenase (FACD) from *Burkholderia* sp. FA1 (UniProt accession Q1JU72) was chemically synthesized (Integrated DNA Technologies) as a sequence optimized to *E. coli* codon usage^[39] and introduced in the pBAD plasmid. Both plasmids were used to transform a One Shot TOP10 *E. coli* strain (Invitrogen). Both strains were grown in LB medium supplemented with ampicillin at 37 °C, and production of DhIA and FACD was induced with 0.008% arabinose when $\text{OD}_{600\text{nm}}$ reached 0.6. The cultures were then incubated for 4 h at 30 °C.

Cells were then pelleted, washed with phosphate buffer saline, mixed in a 1/99 (FACD/DhIA) ratio, and diluted to an $\text{OD}_{600\text{nm}}$ of 0.025 (to reach a 20% droplet occupancy as described before^[41]) in refolding buffer with 1 mg mL^{-1} sodium fluoroacetate, 400 nM purified FluorMango, 700 nM TO1-biotin, 0.1% Pluronic F68 (Sigma), 10 μM Cy5, 200 μg mL^{-1} total yeast RNA (Ambion) and 2 U mL^{-1} proteinase K. The resulting suspension was injected into a droplet generator device and dispersed into 20 μL droplets in Novec 7500 fluorinated oil phase (3 M) containing 3% surfactant to stabilize the emulsion. The emulsion was collected and incubated off-chip for 16 h at 30 °C. Droplets were then reinjected into a sorting device in which they were spaced by a surfactant-free Novec 7500 oil phase, and their red (Cy5, droplet tracer) and green (RNA/TO1-biotin complex) fluorescence was analyzed. Droplets displaying elevated green fluorescence were sorted by applying an electric field (1200 V and 30 kHz). Recovered droplets (as well as a sample of unsorted drops) were transferred into 5 mL LB medium supplemented with ampicillin and incubated for 16 h at 37 °C. Plasmids were recovered using GeneJET Plasmid Miniprep Kit (ThermoScientific) and used to transform fresh One Shot TOP10 *E. coli* strain (Invitrogen), which was grown and induced by arabinose as above. The resulting culture was pelleted, washed with phosphate buffer saline, resuspended in the same buffer, diluted to an $\text{OD}_{600\text{nm}}$ of 0.2, and incubated for 12 h in refolding buffer in the presence of 1 mg mL^{-1} sodium fluoroacetate, 400 nM purified FluorMango, 700 nM TO1-biotin, and 2 U mL^{-1} proteinase K on a microplate reader (SpectraMax iD3, Molecular Devices) set at 28 °C. Green fluorescence ($\lambda_{\text{ex}} = 510$ nm and $\lambda_{\text{em}} = 550$ nm) was then recorded every 10 min. Enrichment was confirmed by qPCR using SsoFast EvaGreen Supermix (Bio-Rad) with 0.2 μM of primers Fwd-FACD and Rev-FACD, or Fwd-DhIA and Rev-DhIA (Table S4, Supporting Information) as recommended by the supplier.

Supporting Information

Supporting Information is available from the Wiley Online Library or from the author.

Acknowledgements

The authors thank Emilie Geersens for fruitful discussions, Marie Vandroux for technical assistance, as well as Sandrine Koechler and Abdelmalek Alioua (IBMP Gene Expression Analysis facility) for technical assistance with high-throughput sequencing. The authors are grateful to Magali Frugier for her critical reading of the manuscript. This work received financial support from the Agence Nationale de la Recherche (DehalofluoridX project ANR-17-CE07-0009 and MICROFLUOR project ANR-21-CE04-0010). This work was performed within the Interdisciplinary Thematic Institute "IMCBio" (ITI 2021–2028 program of University of Strasbourg, CNRS and Inserm), and also supported by IdEx Unistra (ANR-10-IDEX-0002), SFRI-STRAT'US project (ANR-20-SFRI0012), and EUR IMCBio (ANR-17-EURE-0023) under the framework of the French Investments for the Future Program and of the previous LabEx NetRNA (ANR-10-LABX-0036), and also supported by the Centre National de la Recherche Scientifique (CNRS), Université de Strasbourg, and its Initiative of Excellence (IdEx).

Conflict of Interest

The authors declare no conflict of interest.

Data Availability Statement

The data that support the findings of this study are available from the corresponding author upon reasonable request.

Keywords

aptamers, biosensors, defluorinase, droplet microfluidics, fluorescence, fluoride, RNA

Received: August 25, 2022

Revised: October 28, 2022

Published online:

- [1] C. Husser, N. Dentz, M. Ryckelynck, *Small Struct.* **2021**, *2*, 2000132.
- [2] A.-S. V. Bédard, E. D. M. Hien, D. A. Lafontaine, *Biochim. Biophys. Acta, Gene Regul. Mech.* **2020**, *1863*, 194501.
- [3] R. Micura, C. Höbartner, *Chem. Soc. Rev.* **2020**, *49*, 7331.
- [4] A. Ariza-Mateos, A. Nuthanakanti, A. Serganov, *Biochemistry* **2021**, *86*, 962.
- [5] T. Tabuchi, Y. Yokobayashi, *RSC Chem. Biol.* **2021**, *2*, 1430.
- [6] J. Hoetzel, B. Suess, *J. Mol. Biol.* **2022**, *434*, 167631.
- [7] M. Spöring, M. Finke, J. S. Hartig, *Curr. Opin. Biotechnol.* **2020**, *63*, 34.
- [8] W. Thavarajah, M. S. Verosloff, J. K. Jung, K. K. Alam, J. D. Miller, M. C. Jewett, S. L. Young, J. B. Lucks, *npj Clean Water* **2020**, *3*, 18.
- [9] E. Gazzano, L. Bergandi, C. Riganti, E. Aldieri, S. Doublier, C. Costamagna, A. Bosia, D. Ghigo, *Curr. Med. Chem.* **2010**, *17*, 2431.
- [10] S. E. Fenton, A. Ducatman, A. Boobis, J. C. DeWitt, C. Lau, C. Ng, J. S. Smith, S. M. Roberts, *Environ. Toxicol. Chem.* **2021**, *40*, 606.
- [11] H. J. Seong, S. W. Kwon, D.-C. Seo, J.-H. Kim, Y.-S. Jang, *Appl. Biol. Chem.* **2019**, *62*, 62.
- [12] F. Shao, P.-W. Lee, H. Li, K. Hsieh, T.-H. Wang, *Trends Biotechnol.* **2022**, <https://doi.org/10.1016/j.tibtech.2022.06.006>.
- [13] M. S. Frant, J. W. Ross, *Science* **1966**, *154*, 1553.
- [14] M. D. Bygd, K. G. Aukema, J. E. Richman, L. P. Wackett, *mBio* **2021**, *12*, e03001.
- [15] M. D. Bygd, K. G. Aukema, J. E. Richman, L. P. Wackett, *Appl. Environ. Microbiol.* **2022**, *88*, e00288.
- [16] Z. Deng, C. Wang, H. Zhang, T. Ai, K. Kou, *Front Chem* **2021**, *9*, 666450.
- [17] Y. Jiao, B. Zhu, J. Chen, X. Duan, *Theranostics* **2015**, *5*, 173.
- [18] L. Yan, D. Li, Y. Le, P. Dong, L. Liu, *Dyes Pigm.* **2022**, *201*, 110200.
- [19] X. Chen, Z. Huang, L. Huang, Q. Shen, N.-D. Yang, C. Pu, J. Shao, L. Li, C. Yu, W. Huang, *RSC Adv.* **2022**, *12*, 1393.
- [20] J. L. Baker, N. Sudarsan, Z. Weinberg, A. Roth, R. B. Stockbridge, R. R. Breaker, *Science* **2012**, *335*, 233.
- [21] A. Ren, K. R. Rajashankar, D. J. Patel, *Nature* **2012**, *486*, 85.
- [22] W. Thavarajah, A. D. Silverman, M. S. Verosloff, N. Kelley-Loughnane, M. C. Jewett, J. B. Lucks, *ACS Synth. Biol.* **2020**, *9*, 10.
- [23] R. S. Iwasaki, R. T. Batey, *Nucleic Acids Res.* **2020**, *48*, e101.
- [24] Y. Ma, Q. Mou, P. Yan, Z. Yang, Y. Xiong, D. Yan, C. Zhang, X. Zhu, Y. Lu, *Chem. Sci.* **2021**, *12*, 11740.
- [25] M. Ryckelynck, in *RNA Tagging* (Ed: M. Heinlein), Springer, New York, NY **2020**, pp. 73–102.
- [26] F. Bouhedda, A. Autour, M. Ryckelynck, *Int. J. Mol. Sci.* **2017**, *19*, 44.
- [27] T. Gao, Y. Luo, W. Li, Y. Cao, R. Pei, *Analyst* **2020**, *145*, 701.
- [28] P. Swetha, Z. Fan, F. Wang, J.-H. Jiang, *J. Mater. Chem. B* **2020**, *8*, 3382.
- [29] M. You, J. L. Litke, S. R. Jaffrey, *Proc. Natl. Acad. Sci. U. S. A.* **2015**, *112*, E2756.
- [30] J. S. Paige, T. Nguyen-Duc, W. Song, S. R. Jaffrey, *Science* **2012**, *335*, 1194.
- [31] A. Autour, S. C. Y. Jeng, A. D. Cawte, A. Abdolazadeh, A. Galli, S. S. S. Panchapakesan, D. Rueda, M. Ryckelynck, P. J. Unrau, *Nat. Commun.* **2018**, *9*, 656.
- [32] R. J. Trachman, A. Autour, S. C. Y. Jeng, A. Abdolazadeh, A. Andreoni, R. Cojocar, R. Garipov, E. V. Dolgosheina, J. R. Knutson, M. Ryckelynck, P. J. Unrau, A. R. Ferré-D'Amaré, *Nat. Chem. Biol.* **2019**, *15*, 472.
- [33] K. E. Watters, E. J. Strobel, A. M. Yu, J. T. Lis, J. B. Lucks, *Nat. Struct. Mol. Biol.* **2016**, *23*, 1124.
- [34] A. Autour, F. Bouhedda, R. Cubi, M. Ryckelynck, *Methods* **2019**, *161*, 46.
- [35] F. Bouhedda, R. Cubi, S. Baudrey, M. Ryckelynck, *Methods Mol. Biol.* **2021**, *2300*, 203.
- [36] B. A. Prabowo, P. D. Cabral, P. Freitas, E. Fernandes, *Chemosensors* **2021**, *9*, 299.
- [37] L. E. X. Leong, S. Khan, C. K. Davis, S. E. Denman, C. S. McSweeney, *J. Anim. Sci. Biotechnol.* **2017**, *8*, 55.
- [38] C. Donnelly, C. D. Murphy, *Biotechnol. Lett.* **2009**, *31*, 245.
- [39] T. Kurihara, T. Yamauchi, S. Ichiyama, H. Takahata, N. Esaki, *J. Mol. Catal. B: Enzym.* **2003**, *23*, 347.
- [40] D. B. Janssen, F. Pries, J. van der Ploeg, B. Kazemier, P. Terpstra, B. Witholt, *J. Bacteriol.* **1989**, *171*, 6791.
- [41] É. Geersens, S. Vuilleumier, M. Ryckelynck, *ACS Omega* **2022**, *7*, 12039.
- [42] M. A. Boyd, W. Thavarajah, J. B. Lucks, N. P. Kamat, bioRxiv, <https://doi.org/10.1101/2022.03.02.482665>.
- [43] K. Y. Chan, A. B. Kinghorn, M. Hollenstein, J. A. Tanner, *ChemBioChem* **2022**, *23*, 202200006.
- [44] Q. Yu, J. Shi, A. P. K. K. Mudiyansele, R. Wu, B. Zhao, M. Zhou, M. You, *Chem. Commun.* **2019**, *55*, 707.
- [45] J. Abatemarco, M. F. Sarhan, J. M. Wagner, J.-L. Lin, L. Liu, W. Hassouneh, S.-F. Yuan, H. S. Alper, A. R. Abate, *Nat. Commun.* **2017**, *8*, 332.
- [46] M. Ryckelynck, S. Baudrey, C. Rick, A. Marin, F. Coldren, E. Westhof, A. D. Griffiths, *RNA* **2015**, *21*, 458.
- [47] N. B. Leontis, E. Westhof, *RNA* **2001**, *7*, 499.